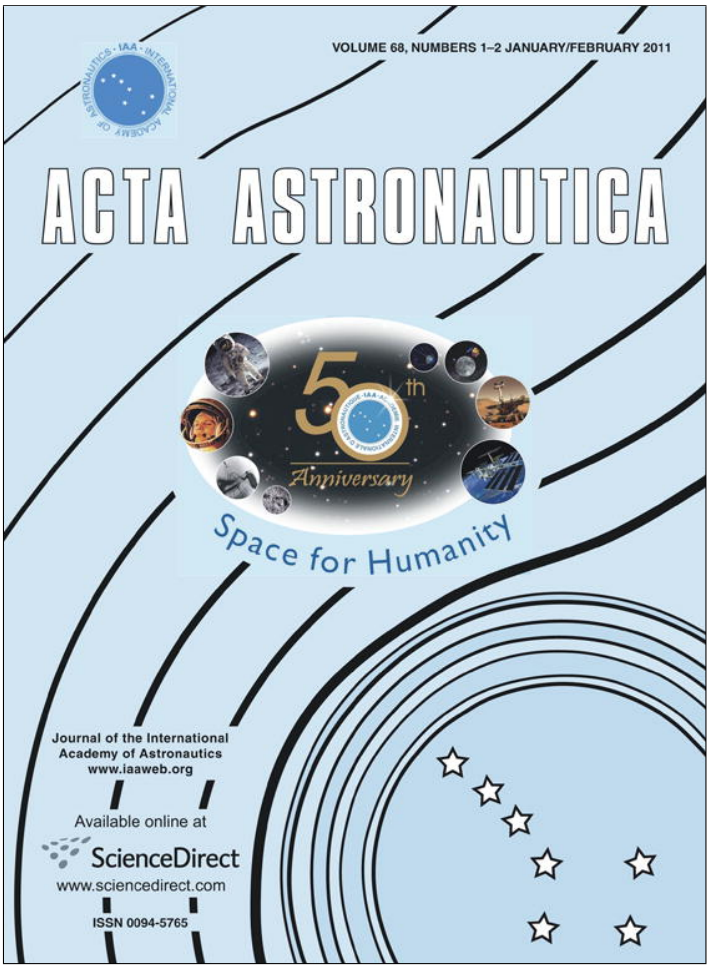


(This is a sample cover image for this issue. The actual cover is not yet available at this time.)

Acta Astronautica 74 (2012) 112–119

Contents lists available at SciVerse ScienceDirect

Acta Astronautica

journal homepage: www.elsevier.com/locate/actaastro

# Numerical simulation of base flow of a long range flight vehicle

S. Saha, S. Rathod, M.S.R Chandra Murty, P.K. Sinha, Debasis Chakraborty *

*Directorate of Computational Dynamics, Defence Research and Development Laboratory, P.O. Box Kanchanbagh, Hyderabad 500058, India*

ARTICLE INFO

*Article history:*
Received 25 October 2011
Received in revised form
7 December 2011
Accepted 9 December 2011

*Keywords:*
Base flow
CFD
Recirculation

ABSTRACT

Numerical exploration of base flow of a long range flight vehicle is presented for different flight conditions. Three dimensional Navier–Stokes equations are solved along with k–$\varepsilon$ turbulence model using commercial CFD software. Simulation captured all essential flow features including flow separation at base shoulder, shear layer formation at the jet boundary, recirculation at the base region etc. With the increase in altitude, the plume of the rocket exhaust is seen to bulge more and more and caused more intense free stream and rocket plume interaction leading to higher gas temperature in the base cavity. The flow field in the base cavity is investigated in more detail, which is found to be fairly uniform at different instant of time. Presence of the heat shield is seen to reduce the hot gas entry to the cavity region due to different recirculation pattern in the base region. Computed temperature history obtained from conjugate heat transfer analysis is found to compare very well with flight measured data.



## 1. Introduction

One of the major aerothermodynamics problems encountered by missiles and satellite launch vehicles during the ascent phase in the atmosphere is the problem of base heating, which is caused due to energy transfer from the rocket exhaust to the vehicle base. With the increase in altitude, the plumes of the rocket motor become more and more underexpanded and bulge in size. This expanding plume interacts with the external stream and cause the hot rocket exhaust recirculates towards the base of the vehicle. Understanding of the mechanism involved in the energy transfer and quantitative estimation of recirculation flow properties are very important for structural and thermal design of base shroud of any missiles. The recirculation flow also changes the base drag and has significant effect on the mission performance. The interaction of rocket exhaust and free stream flow continues to be an active research problem for fundamental flow physics as well as for engineering applications.

Supersonic base flow past an aerospace vehicle continues to be an active research problem for fundamental flow physics as well as for engineering applications. The role of unsteady vortex shedding and large coherent structure in the supersonic base flow is not well understood. Recently, the planar visualization in the experiments of supersonic base flow [1–3] showed evidence of large coherent turbulent structure. The origin of these coherent structures and their impact on the mean flow is far from understood. The base flow features with jet and without jet are shown schematically in Fig. 1(a) and (b). The incoming flow separates at the base shoulder and a shear layer develops. For jet off case, a recompression shock appears, since the flow has to align with the centerline. The streamlines that do not have sufficient energy to overcome the higher pressure downstream of the recompression shock turn back towards the base. The flow features with jet on condition are also similar but the flow has to align with jet axis. The interaction of nozzle boundary layer and the shear layer in the base causes complex recirculation flow, which may not be

* Corresponding author. Tel.: +91 40 24583310;
fax: +91 40 24340037.
*E-mail address:* debasis_cfd@drdl.drdo.in (D. Chakraborty).

0094-5765/$ - see front matter © 2011 Elsevier Ltd. All rights reserved.
doi:10.1016/j.actaastro.2011.12.015

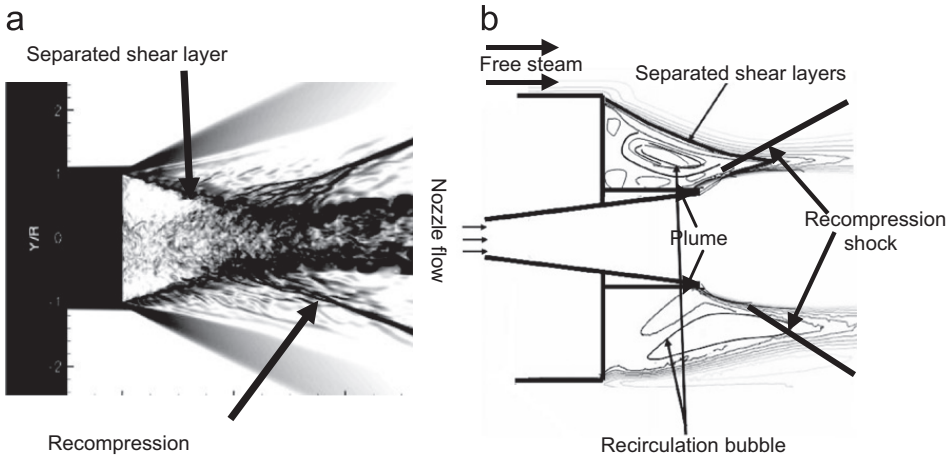


**Fig. 1.** Schematic of Base flow problem: (a) without propulsive jet and (b) with propulsive jet.

symmetrical at the top and the bottom and depends on the pressure ratio of the jet and the free stream flow.

Because of its importance in fundamental flow physics and engineering applications, base flow problems are investigated extensively in the literature. Starting from semi-empirical formulation of Chapman [4], a large number of research papers appeared in freestream—plume interaction on analytical, experimental and numerical methods. Numerical computation of these flows can be very helpful to understand this complex flow phenomena. In fact, most decisive progress in the freestream—plume interaction calculation certainly comes from the solution of the time averaged Navier–stokes equation with turbulence closure [5–11]. Although still costly in computer time, and not always quantitatively satisfactory, this approach allows a truly realistic prediction of the flow field structure. It is also probably the most straightforward way to extend the prediction capability to three-dimensional configuration, whereas the extension of empirical correlation method to three dimensional flows is extremely hazardous and leads to nearly inextricable difficulty. Simpler correlations can predict only one average value of the base flow parameters in the whole region.

Simon et al. [12] reviewed various numerical methods including RANS, DES and LES applied to supersonic base flow. Most of the numerical methods deal with base flow without the presence of nozzle exhaust plume. On engineering application, RANS remain the most popular approach to solve the freestream—plume interaction problem, because of inherent difficulties of the semi empirical procedure as described earlier. Sahu [7] simulated the experimental condition of Herrin and Dutton [13] and predicted the radial variation of base pressure. This study reveals the predicted base pressure with $k$–$\varepsilon$ turbulence model is closer to the experimental value in comparison with other algebraic turbulence models. Chakraborty et al. [9] simulated axisymmetric base flow experiment of Reid and Husting [14] for different pressure ratios of free stream and propulsion jets. A grid adaptive Cartesian mesh based Navier–Stokes solver with $k$–$\varepsilon$ turbulence model was used and a qualitative match of computational base pressures with experimental values was obtained. Bakker et al. [10] simulated the experimental condition of Bannik et al. [15] by conducting two set of numerical simulations; namely, (1) axisymmetric calculation without support sting using a Multidimensional Upwind (MDU) Method [8] and (2) 3D simulation with a coarse grid using Finite – Volume Flux – Difference (LORE) Method [16]. Four different turbulence models namely Spalart Allmaras (SA), $k$–$\omega$, BSL (blending of $k$–$\varepsilon$, $k$–$\omega$) and two equations Shear Stress Turbulence (SST) model were compared for their ability to predict the base pressure. It was observed that two equation models could give reasonable qualitative description of the flow field while SA model could not predict the flow features properly and 3D calculation did not adequately capture the flow features, as observed experimentally. Recently, Dharavath et al. [11] simulated the experimental condition of supersonic base flow conducted at University of Delft, Netherlands by Bannik et al. [15] by solving 3D RANS equations in unstructured mesh using commercial software and brought out the effect of computational grid and turbulence model in predicting the radial variation of base pressure.

In the present work, commercial CFD software CFX TASC flow [17] is used to simulate the interaction of the free stream and rocket exhaust of a long range aerospace vehicle. In the explored configuration, nozzles are flexed for the vehicle control and there exists a small gap between the base shroud and the nozzle. The streamlines in the shear layer between the rocket exhaust and free stream, which do not have sufficient energy to penetrate the higher pressure downstream of the recompression shock could recirculate and enter into the base cavity through the gap. The flow development in the base region including that in the base cavity at various flight instants is analyzed and the predicted temperature history in the base cavity is compared with the values measured in flight.

## 2. Methodology

Commercial CFD software, CFX TASC flow [17] is used for the simulation. It solves 3-D Reynolds Averaged Navier–Stokes (RANS) equation on structured grid based on finite volume approach. It also solves one of the following turbulence models viz. $k$–$\omega$ or SST turbulence model, etc along with the RANS equations. In the present

simulation, $k$–$\varepsilon$ turbulence model is used. The software has four major modules (a) *CFX Build*, imports CAD geometry or creates geometry and generates unstructured volume meshing based on the user input (b) *preprocessor*—sets up the boundary condition and initial field condition (c) *solver manager*—solves the flow field based on the grid and the boundary condition and (d) *postprocessor*—visualizes and extracts the results.

The computational methodology has been validated extensively by comparing the experimental results of supersonic flow past a backward facing step with and without transverse injection [18,19] as well as for supersonic base flows in the presence of propulsive jets and support sting [11]. The details of governing equations, turbulence models and the discretisation schemes are given in the following subsections.

### 2.1. Governing equations

The appropriate system of equations governing the turbulent flow of a compressible gas may be written as:

*Continuity equation*

$$\frac{\partial \rho}{\partial t}+\frac{\partial}{\partial x_k}(\rho u_k)=0, \quad k=1,2,3$$

*Momentum equation*

$$\frac{\partial}{\partial t}(\rho u_i)+\frac{\partial}{\partial x_k}(\rho u_i u_k)+\frac{\partial P}{\partial x_i}=\frac{\partial(\tau_{ik})}{\partial x_k}, \quad i,k=1,2,3$$

*Energy equation*

$$\frac{\partial}{\partial t}(\rho E)+\frac{\partial}{\partial x_k}(\rho u_k H)=-\frac{\partial}{\partial x_k}(u_j \tau_{jk})+\frac{\partial q_k}{\partial x_k}, \quad j,k=1,2,3$$

*Turbulent kinetic energy* ($K$) *equation*

$$\frac{\partial}{\partial t}(\rho k)+\frac{\partial}{\partial x_k}(\rho u_k k)=\frac{\partial}{\partial x_k}\left(\left(\frac{\mu_l}{\mathrm{Pr}}+\frac{\mu_t}{\sigma_K}\right)\frac{\partial k}{\partial x_k}\right)+S_K$$

Rate of dissipation of turbulent kinetic energy ($\varepsilon$) equation

$$\frac{\partial}{\partial t}(\rho \varepsilon)+\frac{\partial}{\partial x_k}(\rho u_k \varepsilon)=\frac{\partial}{\partial x_k}\left(\left(\frac{\mu_l}{\mathrm{Pr}}+\frac{\mu_t}{\sigma_\varepsilon}\right)\frac{\partial \varepsilon}{\partial x_k}\right)+S_\varepsilon$$

where, $\rho$, $u_i$, $p$, $E$, $H$ are the density, velocity components, pressure, total energy and total enthalpy respectively and $\mu=\mu_l+\mu_t$ is the total viscosity; $\mu_l$, $\mu_t$ being the laminar and turbulent viscosity and $Pr$ is the Prandtl number. The source terms $S_k$ and $S_\varepsilon$ of the $K$ and $\varepsilon$ equation are defined as

$$S_K=\tau_{ik}\frac{\partial u_i}{\partial x_k}-\rho\varepsilon \quad \textit{and} \quad S_\varepsilon=C_{\varepsilon 1}\tau_{ik}\frac{\partial u_i}{\partial x_k}-C_{\varepsilon 2}\frac{\rho\varepsilon^2}{K}$$

where turbulent shear stress is defined as

$$\tau_{ik}=\mu_t\left(\frac{\partial u_i}{\partial x_k}+\frac{\partial u_k}{\partial x_i}\right)$$

Laminar viscosity ($\mu_l$) is calculated from Sutherland law as

$$\mu_l=\mu_{ref}\left(\frac{T}{T_{ref}}\right)^{3/2}\left(\frac{T_{ref}+S}{T+S}\right)$$

where $T$ is the temperature and $\mu_{ref}$, $T_{ref}$ and $S$ are known values. The turbulent viscosity $\mu_t$ is calculated as

$$\mu_t=c_\mu\frac{\rho K^2}{\varepsilon}$$

The coefficients involved in the calculation of $\mu_t$ are taken as

$$c_\mu=0.09, \quad C_{\varepsilon 1}=1.44, \quad C_{\varepsilon 2}=1.92$$

$$\sigma_K=1.0, \quad \sigma_\varepsilon=1.3, \quad \sigma_c=0.9$$

Rocket exhaust and air are considered as two different species and their transport equations are solved based on continuum hypothesis. The mixing of these two species (air and rocket exhaust) is considered and mixture viscosity and thermal conductivity are calculated according to Wilke's formula [20] and Saxena's formula [21], respectively.

The heat flux $q_k$ is calculated as $q_k=-\lambda\frac{\partial T}{\partial x_k}$, $\lambda$ is the thermal conductivity.

### 2.2. Discretisation of governing equations

The solver utilizes a finite volume approach, in which the conservation equations in differential form are integrated over a control volume described around a node, to obtain an integral equation. The pressure integral terms in the momentum integral equation and the spatial derivative terms in the integral equations are evaluated using finite element approach. An element is described with eight neighboring nodes. The advective term is evaluated using upwind differencing with physical advection correction. The set of discretised equations form a set of algebraic equations:$A\vec{x}=b$ where $\vec{x}$ is the solution vector. The solver uses an iterative procedure to update an approximated $x_n$ (solution of $x$ at $n$th time level) by solving for an approximate correction $x'$ from the equation $A\vec{x'}=\vec{R}$, where $\vec{R}=\vec{b}-A\vec{x}_n$ is the residual at $n$th time level. The equation $A\vec{x'}=\vec{R}$ is solved approximately using an approach called Incomplete Lower Upper Factorization method. An algebraic multigrid method is implemented to reduce low frequency errors in the solution of the algebraic equations. Maximum residual $(=\varphi_j^{n+1}-f(\varphi_j^{n+1},\varphi_j^n))<10^{-4}$ is taken as convergence criteria.

## 3. Geometry and flow conditions

The base region of the configuration along with the grid distribution is shown schematically in Fig. 2. The annular space between nozzle outer diameter and the vehicle inner diameter is covered with heat shield leaving a small gap, which is used for nozzle flexing. This creates a flow path between ambient and the base cavity. The computational domain is extended $9R$ ($R$=nozzle throat radius) in the downstream direction and $8R$ in the radial direction to capture the plume expansion as well as to satisfy the boundary condition. Computational domain is also extended $5R$ upstream from the nozzle exit and the rocket nozzle domain is taken $2R$ upstream of nozzle throat. Taking the advantage of the symmetry of the geometry, a 20° sector is considered and a multiblock structured grid is generated. As is seen in the figure, grid is very fine near the jet, free stream boundary and the cavity region to capture the formation of

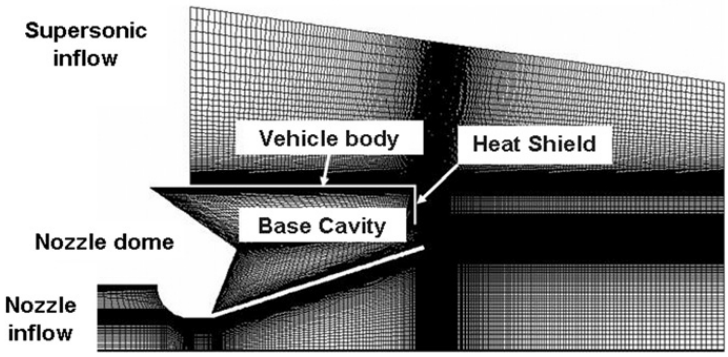


**Fig. 2.** Grid in the computational domain.

**Table 1**
Inflow parameters and rocket exhaust properties.

| Parameters | Time (s) | | |
|---|---|---|---|
| | 40 | 50 | 60 |
| *Free stream parameters* | | | |
| Free stream mach number ($M_\infty$) | 1.3 | 1.8 | 2.6 |
| Ambient pressure($p_\infty$) (KPa) | 46 | 26.5 | 16.4 |
| Ambient temperature, ($T_\infty$) (K) | 261 | 235 | 203 |
| *Rocket exhaust properties* | | | |
| Chamber pressure ($p_0$) (MP)a | 4.4 | 4.1 | 4.5 |
| Chamber temperature ($T_0$) (K) | 3500 | 3500 | 3500 |
| Ratio of specific heat | 1.25 | 1.25 | 1.25 |
| Molecular weight (kg mole/m$^3$) | 26 | 26 | 26 |
| Pressure ratio ($p_j/p_\infty$) | 1.14 | 1.92 | 3.2 |

shear layer and resulting entrainment. The grid independence of the results is established by carrying out three different grids of sizes 0.24, 0.4 and 0.55 millions and comparing the results.

Simulations are carried out for three different time instants and the inflow conditions for the simulations are obtained from the vehicle trajectory. The inflow parameters and the rocket exhaust properties of are summarized in Table 1.

## 4. Results and discussions

As explained earlier, the present simulations contain two inflow boundaries namely; nozzle inflow and free stream inflow. Supersonic inflow conditions are prescribed at free stream inflow, whereas nozzle total pressure and total temperature are prescribed at the nozzle inflow plane. Supersonic outflow, symmetric condition and far field conditions are prescribed at the outflow, symmetry and far field boundary, respectively. Two different species corresponding to rocket exhaust and free stream is considered in the simulation. The Mach number distribution in the symmetry plane presented in Fig. 3 depicts the qualitative features of the flow field in the base region. The nozzle jet is underexpanded with pressure ratio ($p_j/p_\infty$) of 1.92. The bulging of the rocket exhaust, expansion of the free stream flow at base shoulder, shear layer formation at the jet boundary and the recirculation at the base region is clearly visible in the figure. The details of the flow structure in the base region are shown in the exploded view of the velocity vector near the base. A very low speed flow is seen in the base cavity region, which has been explored in detail. The velocity vector (colored with axial velocity, non dimensionalised with $u_{ref}$) and streamline pattern (colored with speed) in the cavity region is shown in Fig. 4. The flow from the shear layer is seen to enter into cavity region and forming a complex recirculation pattern in the base cavity. Four distinct recirculation bubble is seen in the cavity region. The nondimensionalized axial velocity ($u/u_{ref}$) and the temperature distribution ($T/T_\infty$) at the center line of the midplane in the cavity region at 50 s are compared for different grids in Fig. 5(a) and (b), respectively. It is clear that the flow properties are not changing significantly with the change of grids from 0.24 million to 0.55 million thus demonstrating the grid independence of the solutions.

The nondimensionalized temperature distributions at the symmetry plane at different instants ($t$=40, 50 and 60 s) are presented in Fig. 6. With the increase in the altitude, the plume sizes are bulging more and more and causing interaction with the free stream is more intense and also the point of interaction is coming closer to the base. Due to this increase interaction, more and more rocket exhaust is entering into the base cavity. The maximum temperature, minimum temperature and mass fraction of hot rocket exhaust at different instant of time are presented in Table 2. The maximum temperature ($T/T_\infty$) and % of rocket exhaust in the cavity are 2.78 and 8.5% at 40 s while that at 60 s is about 5.57 and 15%, respectively. The rocket exhaust and plume interaction flow field has also been computed based on semi-empirical procedure due to Chapmann [4] and Korst [22], which provide an average value of base pressure and base temperature in the whole base region. The calculated values of base temperature ($T/T_\infty$) and base pressure ($p_b/p_\infty$) at 50 s is 3.51 and 0.57, respectively, which matches qualitatively with CFD values. The gas temperature distribution at the nozzle wall and base shroud wall at different instants of time is shown in Fig. 7(a) and (b). Temperature is seen to be uniform along both the nozzle wall and vehicle inner wall for all the three instants of time. To reduce the entry of the hot gas into the cavity a heat shield is provided at the aft end of the vehicle body in the nozzle exit plane. Effect of the heat shield on the flow parameters in the base region is studied by carrying

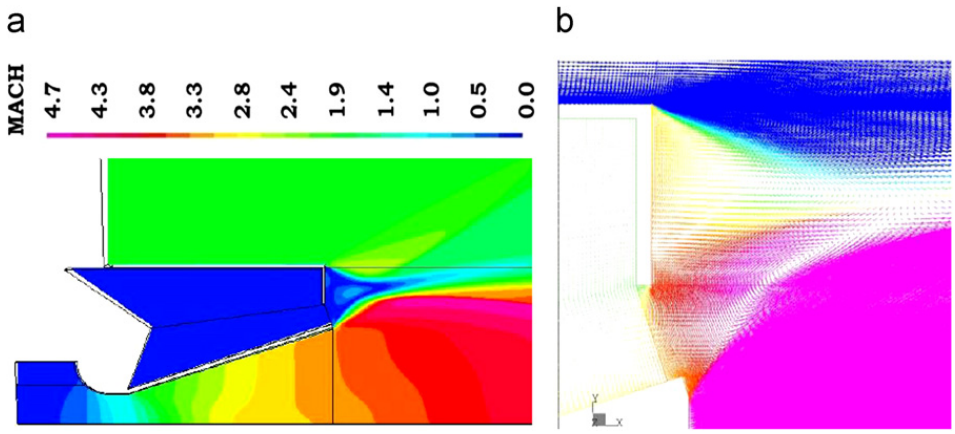


**Fig. 3.** (a) Mach number distribution at symmetry plane at 50 s flight time and (b) exploded view of the velocity vector in the base region.

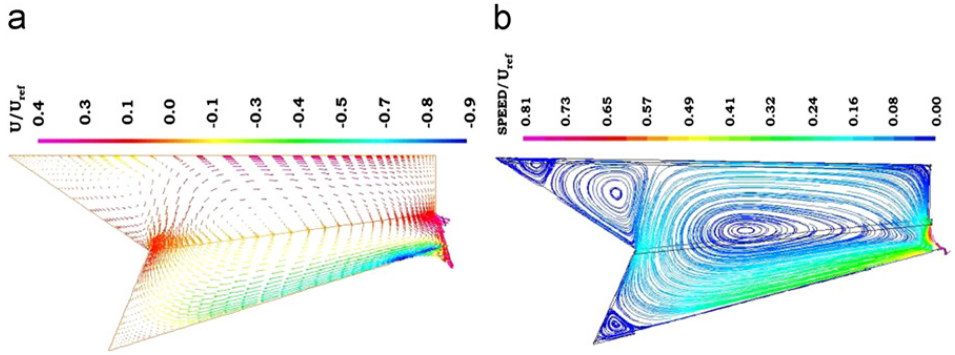


**Fig. 4.** Distribution of: (a) velocity vector and (b) streamline pattern in the base cavity.

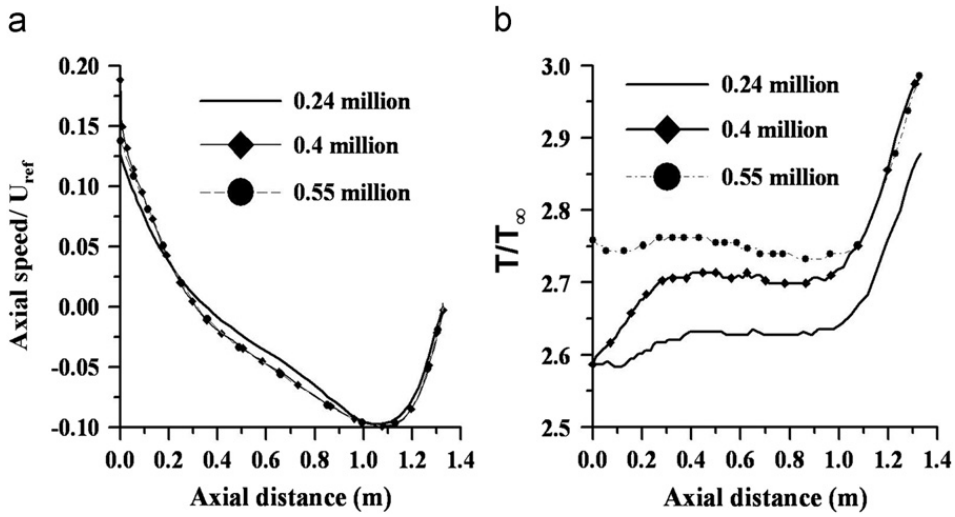


**Fig. 5.** Flow variables in the midplane in the cavity with different grids: (a) axial velocity ($u/u_{ref}$) and (b) temperature ($T/T_{\infty}$).

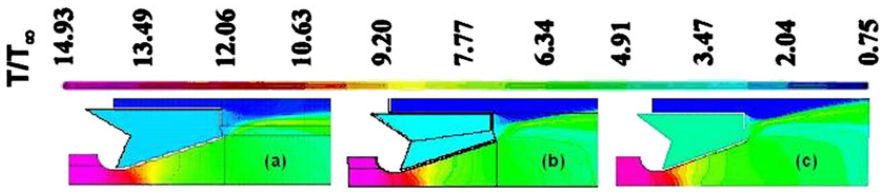


**Fig. 6.** Temperature distribution in the symmetry plane: (a) at 40 s; (b) at 50 s and (c) at 60 s.

out the simulation without the heat shield and comparing the solutions with heat shield case. The temperature distributions on the base shroud wall and nozzle wall in the cavity are compared for with and without heat shield case and are presented in Fig. 8(a) and (b), respectively. Predicted temperature on the cavity walls are higher for without the heat shield case. To find out the reason, streamline plots around the base region for the two cases are compared in Fig. 9. It has been found that for the heat shield case two counter-rotating vortex anchored just downstream of the heat shield whereas in the absence of heat shield, the upper recirculation bubbles entered the cavity. This has caused more entrainment of the hot gas in the cavity.

**Table 2**
Temperature and hot gas mass fraction in the cavity at different time instant.

| Case (s) | Temperature ($T/T_\infty$) | | % of rocket exhaust |
|---|---|---|---|
| | Maximum | Minimum | |
| 40 | 2.78 | 2.71 | 8.5 |
| 50 | 3.62 | 3.45 | 10.5 |
| 60 | 5.57 | 5.32 | 15 |

Many a times, electronics equipments are kept inside the base cavity for vehicle control. Rise of the gas temperature in the cavity due to recirculation flow can adversely affect their performance. It is necessary to have accurate estimation of skin temperature inside the base cavity. A separate conjugate heat transfer analysis is carried out inside the base cavity using the calculated flow profile at the cavity entrance. Computational domain consists of fluid inside the cavity, nozzle, dome, base-shroud and different electronic packages kept inside. Axisymmetric heat conduction equation in the solid domain is solved simultaneously with Navier–Stokes equations in the gas domain in the cavity. User defined function (UDF) is written to impose the flow profiles at different instant of time at the cavity inlet.

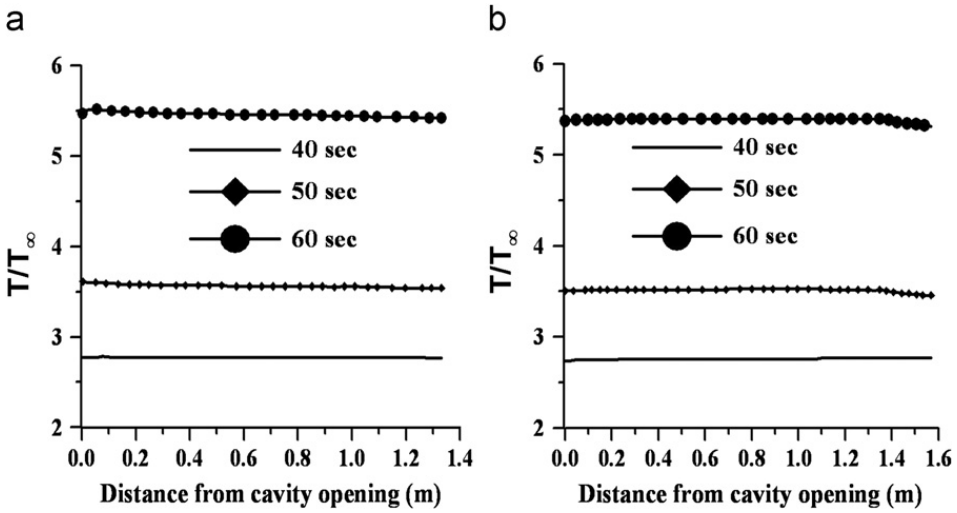


**Fig. 7.** Variation of gas temperature at base cavity at various instants of time: (a) nozzle wall and (b) inner wall of vehicle surface.

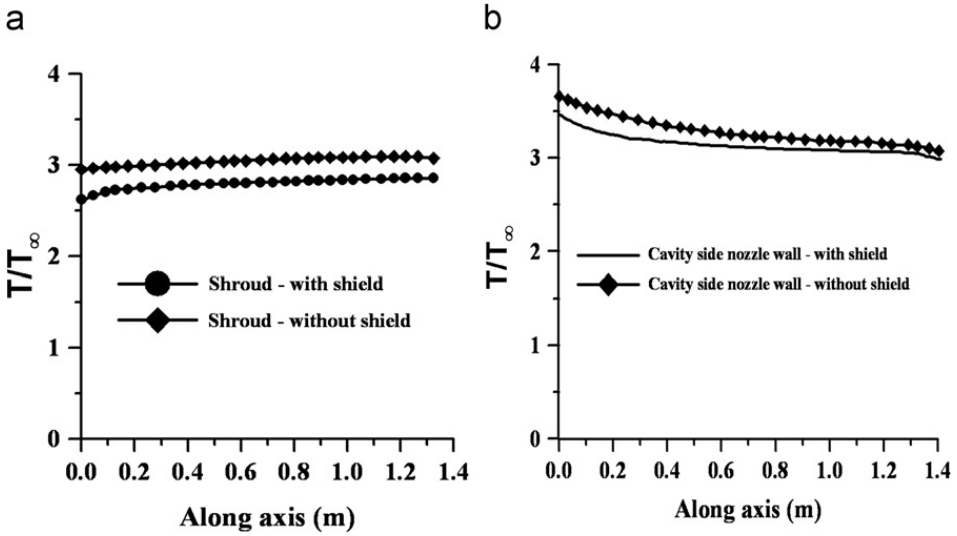


**Fig. 8.** Axial distribution of gas temperature in the cavity at 30 s: (a) nozzle wall and (b) inner wall of vehicle surface.

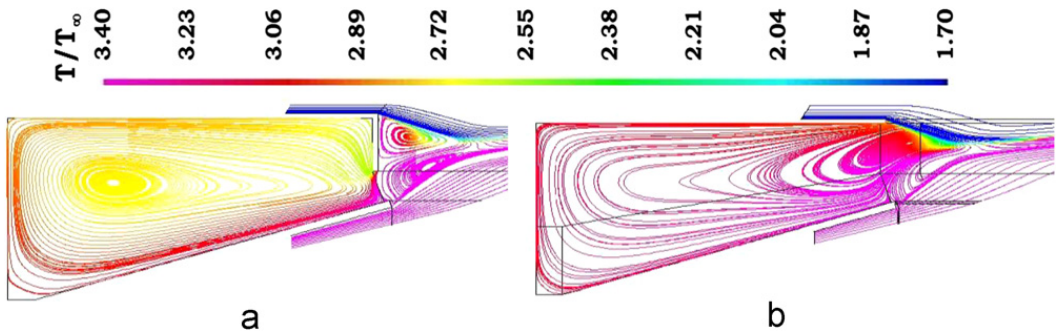


**Fig. 9.** Streamline plot around cavity at 50 s: (a) with heat shield and (b) without heat shield.

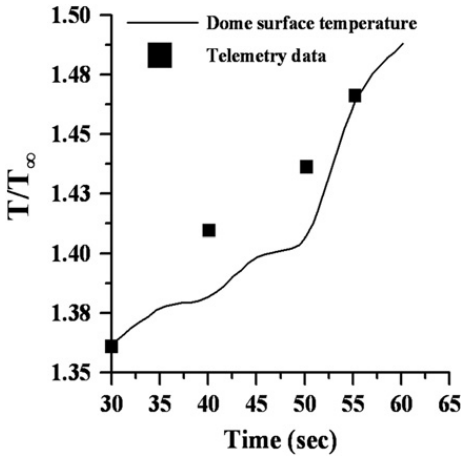


**Fig. 10.** Comparison of cavity skin temperature with flight measurement.

A linear interpolation of the profile has been done in the time instants where flow profile data is not available. The temperature history at the dome is compared with the flight measured temperature in Fig. 10. It can be seen that the trend of temperature increase has been captured very nicely in the computation and predicted temperature is within 1% of the measured value. The rise in temperature in the base cavity is quiet high and is likely to affect the functioning of the various electronic components kept inside. The covering of the base cavity with a flexible thermal boot is advisable to prevent the hot gas to enter the base cavity as well as enable the nozzle to flex for the vehicle control.

## 5. Conclusions

The interaction of rocket exhaust jet and free stream flow at the base region of a long range flight vehicle is simulated numerically for different flight condition. Three dimensional Navier–Stokes equations are shown along with k–$\varepsilon$ turbulence model using commercial CFD software CFX TASC flow. Grid independence of the solution is established by carrying out the simulation of three different grids and comparing the solution. Simulation captured the separation of free stream flow at base shoulder, shear layer formation at the jet boundary, recirculation at the base region and other prominent flow features very crisply. It has been observed that with the increase in altitude, the plume of the rocket exhaust is bulging more and more and the point of interaction between the rocket exhaust and free stream is coming towards the base. Because of this intense interaction, more and more hot gas is entering the base cavity and there is significant increase in gas temperature in the cavity. The velocity and temperature is found to be uniform in the cavity at different instants of time. It has been observed that the presence of the heat shield have reduced the entrainment of hot gas in the cavity region because of the formation of different recirculation pattern in the base region and the predicted temperature in the cavity is higher for without heat shield compared to the heat shield case. The computed base pressure and base temperature matches qualitatively with the available semi empirical procedure. Velocity and temperature distribution at different instants at the cavity entry plane is used to carryout conjugate heat transfer analysis by solving the flow equation in the gas and transient heat conduction equation in the solid. Computed temperature history in the cavity compares very well with flight measured data. It is advisable to cover the base cavity with a flexible thermal boot to prevent the hot gas from entering the base cavity.

## References

[1] C.J. Bourdon, J.C. Dutton, Planar visualizations of large-scale turbulent structures in axisymmetric supersonic separated flows, Phys. Fluids 11 (1) (1999) 201–213.
[2] Bourdon, C.J., Dutton, J.C., Smith, K.M., and Mathur, T., Planar visualizations of large-scale turbulent structures in axisymmetric supersonic base flow, AIAA Paper no. 98-0624.
[3] Bourdon, C.J. and Dutton, J.C., "Visualizations and measurements of axisymmetric base flows altered by surface disturbances," AIAA Paper, no. 2001-0286.
[4] Chapman D.R. "An analysis of base pressure at supersonic velocities and comparison with experiments", NACA Report-1051, 1951.
[5] G.S. Deiwert, Supersonic axisymmetric base flow over boattails containing a central propulsive jets, AIAA J. 22 (1984) 1358–1365.
[6] J. Sahu, C. Nietubicz, J. Steger, Navier–Stokes computations of projectile base flow with and without mass injection, AIAA J. 23 (9) (1985) 1348–1355.
[7] J. Sahu, Numerical computation of supersonic base flow with special emphasis on turbulence modelling, AIAA J. 32 (7) (1994) 1547–1549.
[8] Houtman, E.M., Weide, V.D., Deconinck, E. and Bakker, P.G., "Computational analysis of base flow/jet plume interaction", Proceedings of the Third European symposium on aerothermodynamics for space vehicles, ESA SP-426, pp. 605–612, 1998.
[9] D. Chakraborty, P. Kumar, R. Balu, V. Adimurthy, Numerical simulation of axisymmetric base flow in the presence of propulsive Jet, J. Aeronaut. Soc. India 53 (2001) 35–38.

[10] Bakker, P.G., and Bannink, W.J., Servel, P. and Reijasse,P. "CFD validation for base flows with and without plume interaction", AIAA Paper no. 2002-0438.
[11] M. Dharavath, P.K. Sinha, D. Chakraborty, Simulation of supersonic base flow—effect of grid and turbulence model, Proc. IMechE Part G: J Aerosp. Eng. 224 (2009) 311–319.
[12] F. Simon, S. Deck, P. Guillen., P. Sagant, Reynold-Averaged Navier–Stokes/Large Eddy simulation of supersonic base flow, AIAA J. 11 (2006) 2578–2590.
[13] J.L. Herrin, J.C. Dutton, Supersonic base flow experiments in the near wake of a cylindrical afterbody, AIAA J. 32 (1) (1994) 77–83.
[14] Reid, J., and Hastings, R.C., "The effect of a central jet on the base pressure of a cylindrical After-body in a Supersonic Stream," Aeronautical Research Council (Great Britain) Reports and Memoranda no. 3224, December 1959.
[15] Bannink, W.J., Baker, P.G. and Houtman, E.M., "FESTIP Aerothermodynamics: experimental investigation of base flow and exhaust plume interaction", Memorandum M-775, Aerospace Engineering, Delft University of Technology, 1997.
[16] Walpot, L.M.G.F., "LORE: a 3-D Navier–Stokes solver for high temperature chemical and thermal nonequilibrium Gas flows", Ph.D. Thesis, Aerospace Engineering Department, Delft University of technology, Netherlands.
[17] User Manual, CFX TascFlow 2.11.1, AEA Technology, 2001.
[18] P. Manna, D. Chakraborty, Numerical investigation of transverse sonic injection in a nonreacting supersonic combustor. Proc. Inst. Mech. Eng. Part G: J. Aerosp. Eng. 219 (3) (2005) 205–215, doi: 10.1243/095441005X30261.
[19] P. Manna, D. Chakraborty, Numerical investigation of confinement effect on supersonic turbulent flow past backward facing step with and without transverse injection, J. Aerosp. Sci. Technol. 61 (2) (2009) 283–294.
[20] C.R. Wilke, A viscosity equation for gas mixture, J. Chem. phys. 18 (1950) 517–519.
[21] W.H. Dorrance, Viscous Hypersonic Flow, McGraw Hill, New York, 1962.
[22] H.H. Korst, A theory of base pressure in transonic and supersonic flow, J. Appl. Mech. 23 (1956) 593–600.